

Integrated Approach Using Protein and Ligand Information to Analyze Selectivity- and Affinity-Determining Features of Carbonic Anhydrase Isozymes

Alexander Hillebrecht,^[a] Claudiu T. Supuran,^[b] and Gerhard Klebe^{*[a]}

The application and comparison of selected protein- and ligand-based approaches to elucidate factors important for affinity and selectivity towards the carbonic anhydrase isozymes I, II, and IV are described. Carbonic anhydrases are abundant in pro- and eukaryotes. These enzymes catalyze the reversible hydration of carbon dioxide to bicarbonate and H^+ ions and are thus involved in many important physiological and pathophysiological processes. Due to the fact that the human carbonic anhydrase family consists of 16 closely related isozymes, the design of selective inhibitors is a special challenge for medicinal chemists. In order to extract selectivity-determining features, we applied purely ligand-

based 3D QSAR techniques as well as qualitative comparative molecular field analyses of the targets' binding sites using consensus principal component analysis (CPCA). The dataset for the QSAR studies was deliberately compiled from 1748 inhibitors and comprises about 140 ligands, mainly of the sulfonamide type. Additionally, we employed the novel AFMoC approach, which intrinsically combines protein and ligand information. The simultaneous use of these different techniques gives deeper insight into selectivity and affinity-determining features and provides quantitative models for prediction.

Introduction

Carbonic anhydrases (EC 4.2.1.1, CA) are zinc-containing hydrolases, which catalyze the reversible hydration of carbon dioxide to bicarbonate.^[1,2] In mammals, up to now 16 different isoforms have been characterized. They are involved in a variety of important physiological processes, such as pH and CO_2 regulation, bone resorption, calcification, metabolic reactions, tumorigenicity, and electrolyte secretion.^[3,4] Thus, inhibitors of carbonic anhydrases offer the opportunity to treat several physiological disorders, for example, as drugs against glaucoma, mountain sickness, and epilepsy. Some promising candidates are in clinical and preclinical trials against cancer^[5] or obesity.^[6]


The most important class of CA inhibitors are sulfonamides, showing inhibition constants down to the subnanomolar range.^[7] However, many such compounds lack desirable selectivity towards the target isoform. As a consequence, significant cross-reactivity with other CA isoforms not involved in pathological processes is experienced, leading to undesired side effects, especially for systemically applied compounds. To address the insufficiently resolved selectivity issue, we decided to pursue a comparative approach exploiting both protein and ligand information. The carbonic anhydrases serve as ideal model systems to test the performance of such methods, as the crystal structures of the three isozymes considered in our study are available at good resolution in ligand-free and complexed forms, and affinity data for a broad spectrum of sulfonamide-type inhibitors are available for all three isozymes.

With respect to ligand information, several comparative molecular field analyses have been performed. The popular 3D

QSAR methods CoMFA^[8] (Comparative Molecular Field Analysis) and CoMSIA^[9] (Comparative Molecular Similarity Indices Analysis) correlate spatial field descriptors calculated for mutually aligned ligands with their biological activity. The two methods mainly differ in the functional form to describe distance dependence between the interacting atoms (expressed as energies or similarity indices). The descriptors are correlated with affinity data through PLS^[10] analysis (Partial Least Squares or Projection to Latent Structures), which has the advantage to cope with an adverse relationship of a huge number of highly correlated descriptors to only a few observations. Besides the prediction of affinity data, it is possible to model selectivity in a quantitative manner by considering affinity data with respect to two targets. This can be performed following two alternative approaches: The first method uses differences of pK_i values as independent variables. This procedure has been suc-

[a] A. Hillebrecht, Prof. G. Klebe
Institut für Pharmazeutische Chemie
Philipps-Universität Marburg
Marbacher Weg 6, 35032 Marburg (Germany)
Fax: (+49) 6421 2828994
E-mail: klebe@staff.uni-marburg.de

[b] Prof. C. T. Supuran
Laboratorio di Chimica Bioinorganica
Universita degli Studi di Firenze
Via della Lastruccia 3, 50019 Sesto Fiorentino (Firenze) (Italy)

 Supporting information for this article is available on the WWW under <http://www.chemmedchem.org> or from the author: table of the data set of all ligands used herein. Coordinates of these ligands in SYBYL MOL2 format are available from the authors upon request.

successfully applied in several cases.^[11–13] The second approach derives separate models for each affinity measure^[14–17] and obtains selectivity information by subsequently subtracting the respective pK_i values.

Most crucial in 3D QSAR is the establishment of a meaningful alignment of the studied ligands. Since in our case, protein structures in ligand-free and bound situations are both available to a sufficient number, we decided to include this information in our analysis and consulted the protein structures to generate an alignment.

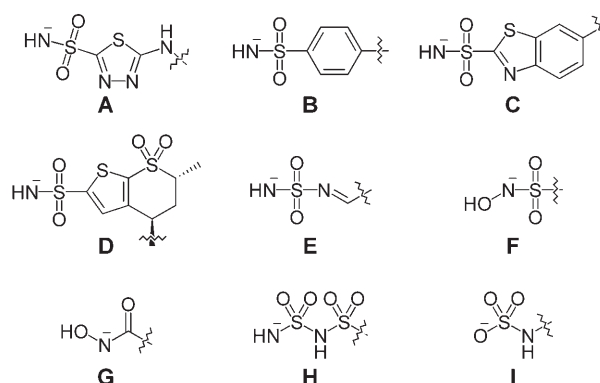
Qualitative selectivity information based on protein data is only available by mapping the interaction properties of active site residues with respect to representative probes using the program GRID.^[18,19] The resulting interaction energies can be analyzed in two ways: either by subtracting the energy values at corresponding grid points, or, more sophisticated, by using a consensus principle component analysis^[20] (CPCA). CPCA, as implemented in GOLPE,^[21] offers the possibility to visualize regions in space that are responsible for a discrimination between the proteins (or families) of interest. Both methods were applied and compared to assess their suitability to elucidate selectivity-determining features.

Since the above-described methods consider either protein or ligand information separately, we additionally used the AFMoC^[22–24] approach (Adaptation of Fields for Molecular Comparison), which merges both sources of information. AFMoC is based on the knowledge-based scoring function DrugScore,^[25–27] which uses distance-dependent pair potentials to identify near-native binding geometries. Moreover, DrugScore turned out to be applicable as an objective function for docking^[28] and to estimate binding affinities.^[29] A knowledge-based scoring function as DrugScore was developed to handle a broad spectrum of structurally deviating proteins. Accordingly, the individual potentials were derived from a large, well-distributed sample set of proteins. Special features present in particular binding sites will be averaged out. A 3D QSAR model, derived for a broad range of different ligands, usually achieves better predictive power than a general scoring function. It has been trained at a very limited range of chemical space, however for the sake of good predictive power if one remains within the scope of the model. AFMoC tries to recover to some degree target specificity by locally weighting the general DrugScore potential values with respect to ligand-binding data of the training set molecules to the target protein. PLS analysis is performed to correlate atom-type specific field contributions with the actual binding affinities (or selectivities) of the embedded ligands. The results obtained by the different methods with respect to selectivity correlation are compared and analyzed by means of graphical visualization.

Target proteins

This study deals with the human carbonic anhydrase (hCA) isoforms carbonic anhydrase I, CA II, and CA IV, which consist in their mature forms of 260, 259, and 266 amino acids, respectively. CA I and II are cytosolic enzymes, while CA IV is bound to the plasma membrane. All three isozymes possess a zinc

ion, coordinated by three histidine residues His94, His96, and His119 (amino acid numbering in the following according to hCA I). The fourth ligand is a water molecule that must be deprotonated for the generation of the catalytically active form. It further hydrogen bonds to the hydroxy group of Thr199. This threonine residue itself forms a hydrogen bond to the neighboring carboxylate moiety of Glu106. The substrate, carbon dioxide, is located in a hydrophobic pocket close to Zn^{II} but not coordinated to it.^[1,30,31] The three conserved histidine residues and zinc together with Thr199 build the basis for the binding of sulfonamides and similar substructures (sulfamates, sulfamides).^[32] The deprotonated inhibitors coordinate to zinc via a negatively charged nitrogen atom,^[1] the remaining hydrogen acting as hydrogen-bond donor to the hydroxy group of Thr199. One of the sulfone oxygen atoms accepts a hydrogen bond from the NH group of Thr199, whereas the other forms an additional polar interaction to the zinc ion. This general binding geometry remains virtually unchanged for the closely related sulfamates (scaffold I, Scheme 1), sulfamides H, or hydroxysulfonamides F. The crystal structures of all three human isozymes have been determined at sufficiently high resolution, and a C α superimposition of the proteins reveals a rather unchanged geometry of the binding pocket, with the exception of His64, which acts as the “proton shuttle” and adopts two alternative conformations.^[33,34]



Scheme 1. Nine different scaffolds contained in the ligand sets used for 3D QSAR studies.

Methods

All molecular modeling and QSAR studies were performed using SYBYL 7.0^[35] (CoMFA and CoMSIA) and DrugScore 1.2 (AFMoC). Chemometric analyses were carried out using GOLPE 4.5.^[21] Several analyses and validation processes were automated using SPL (SYBYL Programming Language) and the scripting language Python. All figures were generated using PyMOL release 0.98.^[36]

Dataset and alignment

A suitable dataset for QSAR has to be structurally sufficiently diverse, yet still representative to provide the desired scope of the derived models.^[37–39] If no common pattern is shared by

the considered molecules, it might be impossible to extract a correlation between the descriptors and the biological activities. This would also make the alignment problem difficult. In a previous study,^[40] we used 87 inhibitors to construct affinity and selectivity models for CA I, II, and IV. However, some of the derived models showed only q^2 values at the border of significance to properly model pK_i differences. Therefore, we tried to profit in the present study from an enlarged data basis and compiled a better distributed and balanced data set. For QSAR studies, the affinity data should spread over a range of at least three logarithmic units^[41] and display approximately an even distribution. In the present study, these requirements are particularly difficult to fulfill, since we have to deal with six dependent variables simultaneously (three pK_i values for the three isozymes and three pairwise differences of the pK_i values (vide infra)). From literature a data set of initially 1748 compounds was selected. These were reduced to a structurally diverse set of 173 ligands^[42–69] using the SELECTOR module of SYBYL (Tanimoto similarities of 2D and atom pair fingerprints). It comprises nine different scaffolds (see Scheme 1). To check the information content of the data with respect to selectivity studies, the correlation coefficient of the affinity data was calculated: a Pearson correlation coefficient of 0.5 for CA I/II and 0.57 for CA I/IV was obtained. For the combination of CA II/IV, however, a rather high degree of correlation ($r=0.86$) indicates that any subsequent conclusion concerning this isozyme pair has to be treated with particular caution.

In 3D QSAR studies, a meaningful alignment of the ligands is of utmost importance. Many different solutions of this problem have been reported, considering either the ligands or proteins as the basis of the alignment rule.^[70,71] Since crystal structures of the proteins under consideration are available, we decided to manually place the molecules into the binding pockets. The X-ray structures 1azm (CA I), 1cil (CA II), and 1znc (CA IV) were retrieved from the Protein Data Bank (PDB)^[72,73] and superimposed by fitting the C^α atoms of conserved amino acids by using the BIOPOLYMER module of SYBYL. Subsequently the ligands and the water molecules were removed with the exception of the four water molecules W301, W325, W394, and W395 in 1cil, since they will most likely remain in the active site upon ligand binding, and their consideration in docking has proved beneficial in earlier studies.^[74] Coordinates of the training-set ligands were converted from 2D to 3D using the program CORINA.^[75] Protonation states were assigned as follows: carboxylic acids were assumed to be deprotonated, whereas nonaromatic amines and amidino groups were considered as protonated. In addition to these standard assumptions, the primary sulfonamide or sulfonate group was also assigned to the deprotonated state, as previously evidenced by NMR.^[1] After calculation of Gasteiger–Marsili charges^[76] the molecules were minimized using the TRIPOS force field^[77] (maximum number of iterations: 1000, minimum gradient: 0.005, default values for the remaining parameters). The ligand geometries thus obtained were matched onto corresponding atoms in the crystal structure references. Once the anchor fragment was superimposed onto the crystal coordinates, the remaining torsions of the ligand were adjusted to achieve maxi-

mal overlap to an appropriate crystal structure template. Finally, to relax the preplaced ligand into an appropriate force-field minimum, the MAB force field^[78] as implemented in MOLOC was used with default settings. During minimization the protein and the zinc anchor of the ligand were kept fixed. Figure 1 shows the alignment of the training set ligands in CA II.

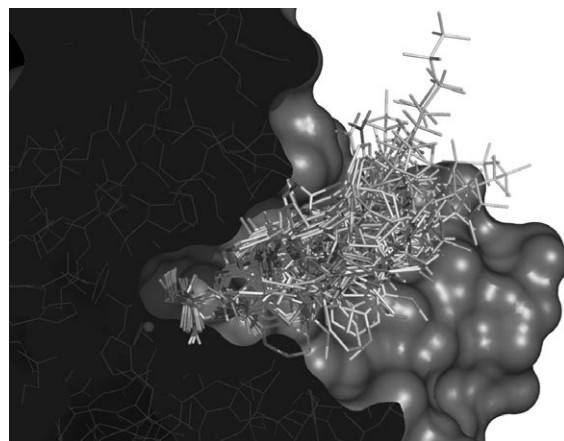


Figure 1. Alignment of the inhibitors used for 3D QSAR studies shown together with the binding site of CA II. The solvent-accessible surface is indicated as a solid surface.

CoMFA and CoMSIA analyses

For CoMFA analysis the interaction energies between a probe atom and the ligand atoms were calculated using a grid box of $26 \times 34 \times 25$ points with 1 Å spacing, embedding all ligands with a margin of at least 4 Å in each direction. The same box dimensions were also used for CoMSIA, GRID, and AFMoC studies. A positively charged sp^3 carbon atom was used as the probe atom for calculating steric and electrostatic CoMFA fields applying SYBYL standard parameters (TRIPOS standard field, dielectric constant $1/r$, cutoff 30 kcal mol⁻¹). CoMSIA fields were computed for steric, electrostatic, hydrophobic, and hydrogen bonding properties, using a probe of charge +1, radius of 1, hydrophobicity and hydrogen bonding properties of +1, and an attenuation factor α of 0.3 for the Gaussian distance-dependent function. All fields were scaled with the CoMFA STD scaling procedure, assigning equal weights to each field. For each of the three alignments affinity values (or affinity differences) were correlated with the field descriptors using SAMPLS^[79] in a leave-one-out cross-validation analysis. Ligands associated with severe uncertainties during alignment or with major singularities in structural terms (especially the class of hydroxamates) were removed from the set, resulting in a collection of 144 ligands. After the optimal number of components was determined, a PLS analysis was performed without cross-validation, applying no column filtering.

In order to further assess the statistical significance of the generated models, we exemplarily performed the following analyses based on the alignment in CA II: a more rigorous cross-validation was carried out by leaving groups of up to

10% of the molecules out, in order to test the stability of the models. Furthermore, all possible field combinations were considered as descriptor variables in various SAMPLS runs in order to check the importance of each field type. To assess whether the models are significant and not the result of chance correlations, the affinity (selectivity) data were scrambled randomly^[80] and subsequently the models were recalculated. This procedure was repeated 100 times for each dependent variable, and mean q^2 values were calculated over all runs; this was done for each of the 10 extracted components.

Finally, the data set was divided into a training set of two thirds and a test set of one third of all ligands. The separation was done using complete linkage clustering of the data set into 48 structurally diverse clusters based on a Tanimoto similarity measure calculated for 2D and atom-pair fingerprints. From each cluster one compound was randomly selected and assigned to the test set, while the remaining molecules were assigned to the training set. After generation of PLS models from the training set, the dependent variables of the test set ligands were predicted and a predictive r^2 value was calculated.

AFMoC analysis

DrugScore pair potentials were calculated for the binding pockets of the three isozymes using the PDB structures 1azm (CA I), 1cil (CA II), and 1znc (CA IV). Location, spacing, and orientation of the grid box as well as the individual ligand alignments were the same as used for CoMFA/CoMSIA analyses. Subsequently, interaction fields were calculated by multiplying the DrugScore potentials with weights derived from Gaussian functions (width $\sigma=0.85$), which were centered at the ligand atom positions. This procedure was performed for eight atom types available in DrugScore: C.3, C.2, C.ar, N.3, N.ar, N.am, O.2, and O.3 (atom type notation similar to the SYBYL atom type conventions). The decision whether to include an individual atom type into the analyses or not was based on the frequency of occurrence of the respective type in the data set, the supposed importance for the protein–ligand interactions, the statistical significance of this atom type in the data set used to derive DrugScore potentials, and some preliminary AFMoC models, based on selected combinations of atom types (data not shown). A value of 10 was taken for the height of the Gaussian repulsive term at short atom–atom distances. The thus obtained interaction fields were correlated with the experimental affinity (differences) using the SAMPLS routine implemented in AFMoC. Statistical performance is assessed by similar parameters as in the other 3D QSAR techniques with the difference that two corresponding sets of parameters are assigned: one refers to the original experimental pK_i value (pK_{i_tot}), the second to a slightly modified pK_i value, pK_{i_PLS} . The pK_{i_PLS} value is obtained by subtracting the mean expected affinity contribution from atom types not considered in the PLS analysis from the original experimental pK_i value. This contribution is estimated according to the original DrugScore potentials by applying the empirically derived scaling factor $c_5^{PAIR} = -1.25e^{-5}$. In total, 167 molecules were used for the generation of the AFMoC models.

As for CoMFA/CoMSIA, some additional statistical tests were accomplished exemplarily for the alignment in CA II. A y -scrambling test was performed in the same way as for CoMFA/CoMSIA, and a leave-five-out analysis was carried out to test the stability of the models.

For all three alignments, the data set was divided into training and test sets analogously to the procedure described above for CoMFA/CoMSIA. The obtained predictive r^2 values served as measure for the predictive power of the AFMoC models.

3D-QSAR-based selectivity maps

In order to visualize the selectivity-determining regions in space, two different options are available, as described above: one is to contour the $stdev*coeff$ maps of the models obtained by employing pK_i differences of two isozymes as independent variables. The second approach is to subtract the $stdev*coeff$ values at corresponding grid points from each other after individual models for two isozymes have been generated. In case of AFMoC the second strategy allows the generation of individual models, each using the protein corresponding to the respective pK_i value. After PLS analysis and subtraction of corresponding $stdev*coeff$ the resulting maps contain selectivity information not only via the affinity values but also by evaluating the two deviating protein environments. Since in the case of the second strategy the models have been built separately, the scale of the $stdev*coeff$ might differ, especially if the similarity of the compared targets is not considerably large. Therefore, it could be advantageous to normalize the values separately before the subtraction. We tried both approaches, and in the case of normalization, we scaled each $stdev*coeff$ field to values between -1 and 1 . All herein described techniques to obtain selectivity maps were applied to CoMFA, CoMSIA, and AFMoC and were compared to each other.

Protein-based selectivity maps

The above-mentioned methods utilize either purely ligand-based information (CoMFA, CoMSIA) or a mixture of both protein and ligand information (AFMoC). A third possibility is to extract knowledge solely from protein structures. The protein structures were superimposed onto 1cil with SYBYL using the C α atoms, and all water molecules and heteroatoms except zinc ions were removed. Only the structures of human wild-type proteins were included in the analyses, namely: 1azm, 1bzm, 1czm, and 1hcb for CA I, 1bcd, 1bn1, 1cil, and 1g1d for CA II, and 1znc for CA IV. The conformation of the most flexible residue, His64, was modeled as the “out” conformation in order to avoid the generation of artefacts at this position. If available, we included several X-ray structures per isozyme to assess the robustness and sensitivity of the methods. As the first step, a grid box of the same dimensions and location as for the 3D QSAR studies was placed into the binding pockets of all three isozymes. Subsequently, the program GRID^[18] was used to calculate the interaction energies between four selected probes and the protein atoms treating non-hydrogen re-

ceptor atoms as rigid (directive $\text{MOVE}=0$). These probes represent four important functionalities of protein–ligand interactions: the DRY probe (hydrophobic, entropic contributions), the C3 probe (hydrophobic, steric contributions), the N1 probe (neutral planar NH, for example, amide, donor function), and the O probe (sp^2 carbonyl oxygen, acceptor function). To extract information from the obtained descriptors relevant for selectivity between two proteins, we tested two approaches: the first simply subtracts the energy values of two corresponding grid points from each other and the resulting differences are used for the contour maps. The second is to perform a consensus principal component analysis (CPCA)^[20] as implemented into the program GOLPE.^[21] The calculated GRID fields were imported into GOLPE and pretreated in the following way: first a maximum cutoff of 0 kcal mol^{-1} was applied in order to focus on favorable interactions only, following the recommendations of several authors.^[20,81] Then, all data points with an absolute value smaller $0.01 \text{ kcal mol}^{-1}$ or a standard deviation below $0.02 \text{ kcal mol}^{-1}$ were set to zero. Furthermore, 2- and 3-level variables (that is, variables taking on only two or three distinct values over the entire matrix) were discarded, and the “cut-out tool” was used to remove all data points from the following analyses which had a distance beyond 4.5 \AA from an artificial “ligand”, which was constructed in a way to sufficiently cover the entire binding sites of the enzymes. Block unscaled weights (BUW) were applied in order to give all four probes the same initial importance in the CPCA models. Three principal components were extracted, and so-called “active CPCA differential plots” were visualized and interpreted for each of the four probes. This type of plot allows the user to draw a vector between two objects in the scores plot for a distinct probe. GOLPE displays in an associated plot the selectivity fields calculated from the differences of the scores of the objects at the ends of the drawn vector.

Results and Discussion

Statistical results

The molecular alignments of the inhibitors generated for the three different isozymes were rather similar. Figure 1 shows the alignment of the inhibitors in the cavity of CA II. Supposedly, in this enzyme the most reliable superposition could be achieved relative to the other two isozymes, since 60 CA II crystal structures with bound inhibitors were available as reference, while for the other two cases only three (CA I) or one (CA IV) templates could be extracted from the PDB.

Table 1 shows the statistical results for all CoMFA, CoMSIA, and AFMoC analyses with individual pK_i values as independent variables using all three separate alignments. The q^2 values of all models are greater than 0.3, indicating their statistical significance.^[80] Moreover, almost all q^2 values are above 0.5, except for the CoMFA and AFMoC models for CA I, if the alignment generated in CA I or CA IV is used. In general, the prediction of the pK_i value of CA I seemed to be affected by larger residual errors than for CA II and IV. Most of the remaining models show excellent statistical significance, indicated by q^2 values

above 0.6. Interestingly, the ligand alignment in CA II exhibits the highest q^2 values for most of the cases, irrespective of which set of pK_i values is predicted. Several factors might explain this finding: the ligand alignment in CA II is supported by a large number of crystal structures, whereas for the others only a few reference structures are available. Furthermore, the finally accepted superposition in each binding pocket revealed only minor differences. In general, it has been suggested that 3D QSAR models perform better if the ligands are superimposed in a highly consistent way.^[82,83] As a more rigorous test of the stability of our models, a cross-validation with leave-10%-out was performed, where the data set is divided into ten groups of equal size. Each group is left out once during cross-validation, and the q^2 value is calculated. If the obtained q^2 values significantly decrease in comparison to those of a leave-one-out analysis (LOO analysis), the models are probably unstable (as obviously the large LOO q^2 value is only revealed due to a high degree of redundancy in the data set).^[84] The medium decrease in q^2 for CoMFA was 0.02 and for CoMSIA 0.01, confirming the robustness of the models. For AFMoC, a leave-five-out analysis was carried out yielding average differences between LOO q^2 and leave-five-out q^2 of 0.02 for both q^2_{tot} and q^2_{PLS} .

The statistics for the models obtained with pK_i differences are shown in Table 2. For these models in all cases q^2 values above 0.5 could be obtained, demonstrating the significance also of the selectivity models. The dependence of the performance on the alignment is small, as for the individual affinity values, and the alignment in CA II yields in almost all cases the highest q^2 value as well. Nevertheless, one has to bear in mind that the dependent variable in this case is a *difference* of two individual variables and is therefore affected by an error in the magnitude of the sum of the single variables' errors, due to the laws of error propagation.

We also examined another approach to predict selectivity, where the differences between pK_i values are calculated from the pK_i predictions of the individual models. The statistical parameters are shown in Table 3. Compared to the approach using the pK_i differences as independent variable, in most cases this method performs virtually identically well. The difference in the respective q^2 of the two approaches is mostly below 0.05 except for the AFMoC selectivity models for CA II and CA IV. For all 3D QSAR techniques used herein, this selectivity property was the most difficult to predict. This is not unexpected due to the high initial correlation of the target-specific pK_i values.

As outlined by many authors, the predictive r^2 value is the most informative parameter to assess the external predictive power of QSAR models.^[37,82,84,85] It reflects best the “real life” situation if compounds are predicted which were not included in the process of model derivation. However, in our studies the trends revealed by the q^2 are also present in the predictive r^2 values, as shown in Tables 1, 2, and 3. The CoMSIA approach showed best performance in almost all cases, while CoMFA performed slightly worse. For the major part of pK_i (difference) predictions, predictive r^2 values clearly above 0.5 could be achieved, finally proving the predictive power of the models. In

Table 1. Statistical results of CoMFA, CoMSIA, and AFMoC^[a] analyses of the affinity data using three alignments.

	CoMFA	pK _i I CoMSIA	AFMoC ^[b]	CoMFA	pK _i II CoMSIA	AFMoC ^[b]	CoMFA	pK _i IV CoMSIA	AFMoC ^[b]
Alignment in CA I									
q^2	0.449	0.530	0.466 (0.423)	0.779	0.840	0.820 (0.806)	0.704	0.777	0.760 (0.752)
s_{PRESS}	0.789	0.728	0.808 (0.808)	0.615	0.522	0.542 (0.542)	0.684	0.591	0.605 (0.605)
r^2	0.848	0.862	0.651 (0.623)	0.922	0.918	0.913 (0.906)	0.907	0.895	0.863 (0.858)
S	0.414	0.395	0.653 (0.653)	0.366	0.374	0.378 (0.378)	0.384	0.405	0.458 (0.458)
F	154.448	172.230	75.380 (66.830)	325.628	387.312	278.600 (256.700)	268.029	297.668	202.500 (194.500)
no.comp.	5	5	4	5	4	6	5	4	5
$r^2_{\text{pred.}}$	0.345	0.508	0.180	0.746	0.816	0.781	0.735	0.776	0.652
Alignment in CA II									
q^2	0.530	0.580	0.492 (0.469)	0.853	0.860	0.791 (0.784)	0.825	0.819	0.755 (0.754)
s_{PRESS}	0.731	0.689	0.787 (0.787)	0.504	0.489	0.580 (0.580)	0.529	0.534	0.612 (0.612)
r^2	0.909	0.860	0.635 (0.618)	0.949	0.943	0.858 (0.853)	0.961	0.935	0.854 (0.854)
S	0.322	0.397	0.667 (0.667)	0.297	0.313	0.480 (0.480)	0.249	0.321	0.472 (0.472)
F	227.980	169.634	70.480 (65.500)	423.840	453.478	244.000 (234.500)	482.752	395.208	188.800 (187.800)
no.comp.	6	5	4	6	5	4	7	5	5
$r^2_{\text{pred.}}$	0.423	0.499	0.219	0.767	0.825	0.658	0.772	0.779	0.663
Alignment in CA IV									
q^2	0.435	0.512	0.385 (0.367)	0.822	0.851	0.753 (0.743)	0.749	0.785	0.709 (0.705)
s_{PRESS}	0.798	0.742	0.864 (0.864)	0.552	0.504	0.631 (0.631)	0.630	0.581	0.665 (0.665)
r^2	0.845	0.851	0.526 (0.513)	0.935	0.931	0.825 (0.818)	0.920	0.920	0.790 (0.786)
S	0.418	0.410	0.758 (0.758)	0.333	0.343	0.531 (0.531)	0.356	0.355	0.565 (0.565)
F	150.393	157.381	60.390 (57.250)	398.011	466.890	191.100 (182.500)	317.495	397.606	151.900 (149.100)
no.comp.	5	5	3	5	4	4	5	4	4
$r^2_{\text{pred.}}$	0.402	0.513	−0.091	0.838	0.833	0.590	0.792	0.784	0.450

[a] For calculation of DrugScore fields, the same protein as taken for the alignment was used. [b] The first value refers to the PLS models using pK_i_tot, the second value in parentheses refers to pK_i_PLS (for explanation, see text).

general, poorest predictivity was encountered for the models of CA I affinities and the selectivity between CA II and IV. AFMoC was also able to produce robust estimates of most of the dependent variables, though with decreased performance compared to the other two 3D QSAR approaches. The optimum mixing factor for each model was determined to be 1.0 in all cases. The reduced performance of AFMoC compared to the purely ligand-based approaches may be explained by the huge amount of ligand information provided by the large size of the data sets. Obviously, these data sufficiently cover the relevant aspects of the underlying structure–activity (–selectivity) relationships, such that the incorporation of protein information does not improve the predictive power of the models. This is also in accordance with the finding that a mixing factor of 1.0 is optimal for all models, meaning that a maximum of ligand information yields the best results.

In order to assess that no chance correlations were responsible for the results, a y-randomization test was carried out exemplarily for the alignment produced in CA II, because it yielded the best models. The mean q^2 values, averaged over 100 runs, were negative without exception, confirming the relevance of our models.

Visualization of the property maps

One prominent feature of 3D QSAR methods is the possibility to visualize the regions in space that are responsible for an increase or decrease of a particular type of dependent variable, thus providing additional information about the structure–activity and –selectivity relationship. Contours are drawn around those grid points where the coefficient of the QSAR equation multiplied with the standard deviation of the corresponding

Table 2. Statistical results of CoMFA, CoMSIA, and AFMoC^[a] analyses of the selectivity data using ΔpK_i as dependent variables and three alignments.

	CoMFA	pK_i I– pK_i II CoMSIA	AFMoC ^[b]	CoMFA	pK_i I– pK_i IV CoMSIA	AFMoC ^[b]	CoMFA	pK_i II– pK_i IV CoMSIA	AFMoC ^[b]
Alignment in CA I									
q^2	0.734	0.744	0.601 (0.637)	0.725	0.711	0.628 (0.652)	0.546	0.606	0.532 (0.585)
s_{PRESS}	0.622	0.608	0.763 (0.763)	0.591	0.603	0.665 (0.665)	0.449	0.416	0.452 (0.452)
r^2	0.963	0.941	0.801 (0.819)	0.948	0.910	0.814 (0.826)	0.871	0.814	0.727 (0.758)
S	0.231	0.292	0.539 (0.539)	0.256	0.336	0.470 (0.470)	0.239	0.287	0.345 (0.345)
F	511.084	364.159	129.600 (145.800)	418.786	280.285	140.700 (152.700)	186.524	151.599	85.800 (101.000)
no.comp.	7	6	5	6	5	5	5	4	5
$r^2_{pred.}$	0.678	0.741	0.530	0.670	0.683	0.580	0.492	0.568	0.461
Alignment in CA II									
q^2	0.758	0.786	0.668 (0.688)	0.709	0.737	0.649 (0.663)	0.741	0.667	0.574 (0.618)
s_{PRESS}	0.598	0.552	0.701 (0.701)	0.609	0.575	0.646 (0.646)	0.343	0.383	0.431 (0.431)
r^2	0.977	0.950	0.879 (0.886)	0.959	0.911	0.822 (0.829)	0.958	0.838	0.729 (0.757)
S	0.184	0.368	0.423 (0.423)	0.230	0.334	0.460 (0.460)	0.139	0.267	0.344 (0.344)
F	633.455	330.962	164.700 (177.100)	451.192	283.130	148.800 (156.300)	380.763	179.450	86.510 (100.200)
no.comp.	9	4	7	7	5	5	8	4	5
$r^2_{pred.}$	0.718	0.791	0.616	0.602	0.741	0.531	0.524	0.565	0.564
Alignment in CA IV									
q^2	0.673	0.735	0.634 (0.650)	0.719	0.720	0.633 (0.643)	0.627	0.636	0.534 (0.539)
s_{PRESS}	0.686	0.617	0.734 (0.734)	0.599	0.593	0.660 (0.660)	0.408	0.400	0.450 (0.450)
r^2	0.897	0.926	0.803 (0.812)	0.949	0.918	0.765 (0.771)	0.912	0.852	0.641 (0.645)
S	0.384	0.325	0.538 (0.538)	0.254	0.321	0.528 (0.528)	0.198	0.255	0.394 (0.394)
F	240.781	347.646	108.700 (115.000)	364.547	308.742	104.900 (108.500)	237.330	199.734	72.430 (73.730)
no.comp.	5	5	6	7	5	5	6	4	4
$r^2_{pred.}$	0.705	0.755	0.470	0.721	0.728	0.421	0.528	0.609	0.110

[a] For calculation of DrugScore fields, the same protein as taken for the alignment was used. [b] The first value refers to the PLS models using pK_i _tot, the second value in parentheses refers to pK_i _PLS (for explanation, see text).

descriptor column (stdev*coeff) is above or below a user-defined threshold. Some of the maps reflect properties mirrored by the receptor, but it has to be pointed out that this is not necessarily the case, since—for CoMFA and CoMSIA—only ligand information is evaluated to derive the models or—as in the present study—also for AFMoC plays the dominant role due to the size and scope of the data set. All CoMSIA maps shown are generated by PLS analysis of the pK_i differences, using the alignment in CA II. The AFMoC selectivity maps were obtained performing PLS analyses for each pK_i value separately using the corresponding protein and calculating the differences of the QSAR coefficients afterwards. Also in this case only the ligand alignment in CA II was used.

Figure 2A shows the steric CoMSIA contour map of the selectivity model, built on the differences of the pK_i values of CA I and CA II. The catalytic zinc ion (magenta sphere) as well

as selected amino acid residues of CA I (green) and CA II (orange) are depicted. The green isopleth indicates a region where steric bulk increases the selectivity towards CA I, while sterically demanding substituents occupying the orange regions increase selectivity towards CA II. Additionally, the inhibitors **1** ($\Delta pK_i(I-II) = -2.60$, brown) and **2** ($\Delta pK_i(I-II) = 0.86$, gray) are displayed as examples for ligands with a preference to inhibit CA I or CA II, respectively (Scheme 2). It has to be noted that the “preference” for a distinct isozyme is only considered relative to the range and distribution of the respective pK_i difference. For example, a compound (like **2**) with a $\Delta pK_i(I-II)$ value of 0.86 cannot be termed “highly selective” for CA I from a medicinal chemistry point of view, but in comparison to other entries in the dataset, it shows a higher tendency to bind to CA I. The green contour is mostly occupied by molecular portions present in scaffold **H** (see Scheme 1). This com-

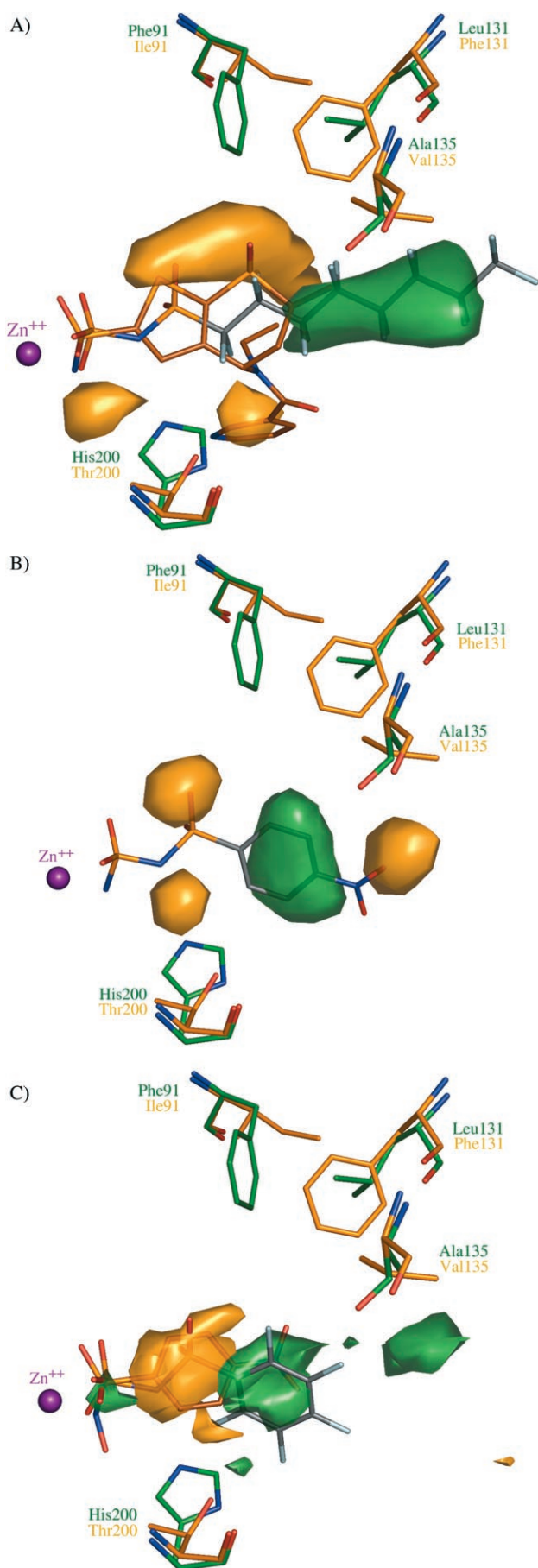
Table 3. Statistical results of CoMFA, CoMSIA, and AFMoC^[a] analyses of the selectivity data built from individual affinity models using three alignments.

	CoMFA	pK _i I–pK _i II CoMSIA	AFMoC ^[b]	CoMFA	pK _i I–pK _i IV CoMSIA	AFMoC ^[b]	CoMFA	pK _i II–pK _i IV CoMSIA	AFMoC ^[b]
Alignment in CA I									
q^2	0.687	0.728	0.646 (0.646)	0.693	0.695	0.614 (0.614)	0.544	0.596	0.432 (0.432)
s_{PRESS}	0.671	0.625	0.722 (0.722)	0.621	0.619	0.676 (0.676)	0.451	0.422	0.499 (0.499)
r^2	0.892	0.908	0.767 (0.767)	0.897	0.886	0.741 (0.741)	0.864	0.806	0.662 (0.662)
S	0.395	0.363	0.585 (0.585)	0.359	0.379	0.554 (0.554)	0.246	0.293	0.385 (0.385)
F	221.989	267.807	85.789 (85.789)	236.056	209.833	91.582 (91.582)	172.344	141.283	50.866 (50.866)
no.comp.	5	5	6	5	5	5	5	4	6
$r^2_{\text{pred.}}$	0.571	0.728	0.489	0.544	0.467	0.453	0.445	0.570	0.462
Alignment in CA II									
q^2	0.731	0.775	0.678 (0.678)	0.702	0.738	0.639 (0.639)	0.702	0.641	0.495 (0.495)
s_{PRESS}	0.624	0.569	0.684 (0.684)	0.616	0.574	0.654 (0.654)	0.367	0.400	0.469 (0.469)
r^2	0.935	0.927	0.786 (0.786)	0.944	0.911	0.734 (0.734)	0.886	0.869	0.701 (0.701)
S	0.307	0.325	0.580 (0.580)	0.267	0.334	0.562 (0.562)	0.227	0.241	0.361 (0.361)
F	316.049	340.394	132.604 (132.604)	320.227	277.463	88.346 (88.346)	148.199	179.265	74.905 (74.905)
no.comp.	6	5	4	7	5	5	7	5	5
$r^2_{\text{pred.}}$	0.756	0.771	0.533	0.711	0.651	0.583	0.600	0.480	0.405
Alignment in CA IV									
q^2	0.664	0.728	0.656 (0.656)	0.697	0.704	0.655 (0.655)	0.589	0.584	0.478 (0.478)
s_{PRESS}	0.695	0.625	0.707 (0.707)	0.618	0.610	0.638 (0.638)	0.428	0.429	0.476 (0.476)
r^2	0.898	0.910	0.733 (0.733)	0.897	0.896	0.730 (0.730)	0.853	0.824	0.596 (0.596)
S	0.382	0.359	0.622 (0.622)	0.360	0.361	0.564 (0.564)	0.256	0.279	0.419 (0.419)
F	283.942	273.300	109.812 (109.812)	234.915	233.030	108.137 (108.137)	156.803	159.045	58.953 (58.953)
no.comp.	5	5	4	5	5	4	5	4	4
$r^2_{\text{pred.}}$	0.610	0.765	0.554	0.559	0.725	0.444	0.532	0.550	0.487

[a] For calculation of DrugScore fields, the same protein as taken for the alignment was used. [b] The first value refers to the PLS models using pK_i_tot, the second values in parentheses refers to pK_i_PLS (for explanation, see text).

pound class shows highest preference for the isozyme CA I, and most of the CA I-selective regions are associated with that class. In CA I, the residues Leu131 and Ala135 open up a larger space for sterically demanding moieties compared to Phe131 and Val135 in CA II. The large orange contour in Figure 2A indicates a CA II-selective region, where especially the oxygen atoms of the endocyclic sulfone group of the thienothiopyranes (scaffold **D**, for example, compound **1**) is frequently found. The active site of CA II exhibits here an isoleucine residue (Ile91), whereas in CA I a phenylalanine reduces the available space. The two smaller orange contours can be related to the exchange of His200 (CA I) by Thr200 (CA II). Some of the CA II-selective thienothiopyranes (such as **1**) possess larger substituents at their amino group, which point into the right contour.

The hydrophobic CoMSIA contours are shown in Figure 2B together with compound **3** ($\Delta pK_i(\text{I–II})=0.60$, gray) using the same color coding. In this case no obvious correlation of the amino acid composition of the active site residues and the presence of these contours can be established, presumably because entropic and desolvation effects play a predominant role for binding (for example, the green contour next to the phenyl ring of **3**). Such properties can be important for ligand binding and require hydrophobic regions on the ligand surface, however they do not necessarily reflect intimate correspondence on the side of the protein binding pocket. Also the orange contour, enclosing the second sulfone group not being part of the zinc anchor, reflects the preference of this inhibitor class for CA I: the presence of hydrophobic moieties in that area enhances CA II selectivity, while hydrophilic moieties provoke CA I selectivity. One of the remaining orange contours marks a posi-

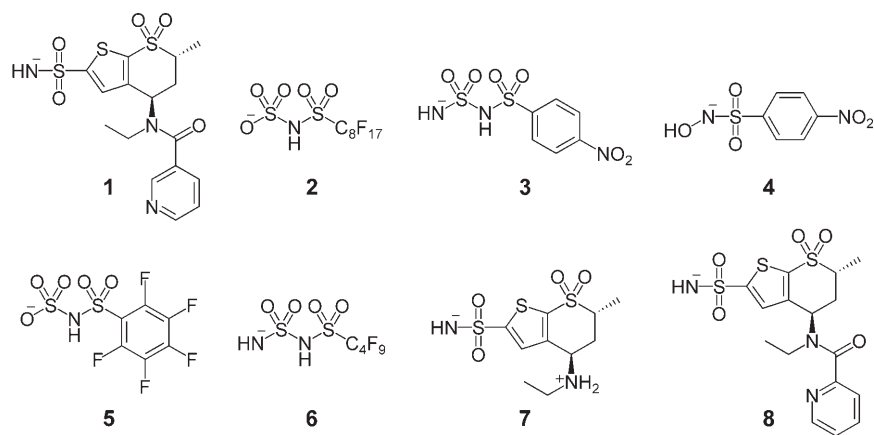


tion where several ligands with scaffold **H** possess polar groups, such as the oxygen atoms of the nitro group of **3**. Obviously such groups are detrimental for CA II binding but enhance selectivity towards CA I.

The steric and hydrophobic property maps were selected in order to compare the CoMSIA contours to the corresponding AFMoC maps. As the AFMoC approach is based on atom types rather than on generic properties, the fields of several atom types corresponding best to the considered CoMSIA properties have to be combined to enable such a comparison. In the present case we merged the C.3, C.2, and C.ar fields. They are displayed in Figure 2C together with the hydroxysulfonamide **4** ($\Delta pK_i(\text{I-II}) = -3.80$, brown) and compound **5** ($\Delta pK_i(\text{I-II}) = 1.38$, gray), applying the same color coding as before. The larger green contour around the phenyl ring of **5** coincides well with the respective hydrophobic CoMSIA contour (Figure 2B). AFMoC marks a region occupied by the phenyl ring of **4** as CA II-selective, which is in accordance with the steric and hydrophobic CoMSIA maps at that location. The small orange fragment close to His200 also finds its counterpart in the steric CoMSIA map (Figure 2A).

As another example for mutually corresponding CoMSIA and AFMoC maps, the selectivity models between CA I and CA IV are discussed, considering properties (or atom types, respectively), which are related to directed interactions. Figure 3 presents the acceptor CoMSIA map (part A) and the O.2 AFMoC map (part B) together with the catalytic zinc ion and inhibitors **6** ($\Delta pK_i(\text{I-IV}) = 1.15$, gray) and **7** ($\Delta pK_i(\text{I-IV}) = -3.05$, brown). Green contours highlight regions where the presence of an acceptor (or O.2 atom) enhances CA I selectivity, magenta contours indicate areas where the occurrence of an acceptor (or O.2 atom) increases selectivity towards CA IV. As in the previous case, it has to be noted that the correspondence of the selected maps of both approaches is not perfect. Also other atom types beside O.2 (such as O.3, N.ar) can act as acceptors, but O.2 is the most frequently occurring atom type with clear monofunctional acceptor properties in this data set. The green contour (Figure 3A) close to the sulfone oxygen atoms of **6** is present in the CoMSIA map only and can be attributed to a CA I preference found for scaffold **H**. However, these oxygen atoms do not form hydrogen bonds to CA I. Since CoMSIA only evaluates ligand information, it simply reflects the observation that ligands with acceptors in this region possess CA I preference in a phenomenological way. On the other hand the

Figure 2. A) Steric and B) hydrophobic stdev*coeff CoMSIA and C) combined C.2, C.3, and C.ar AFMoC contour maps for CA I/II selectivity. The catalytic zinc ion (violet sphere) is shown as well as selected amino acids of CA I (green) and CA II (orange); hydrogen atoms are omitted for clarity. A) Green contours (level: 0.002) indicate regions enhancing selectivity towards CA I, orange contours (level: -0.0005) show areas enhancing selectivity towards CA II. For reference, inhibitors **1** ($\Delta pK_i(\text{I-II}) = -2.60$, brown) and **2** ($\Delta pK_i(\text{I-II}) = 0.86$, gray) are depicted. B) Green contours (level: 0.004) indicate regions enhancing selectivity towards CA I, orange contours (level: -0.0033) show areas enhancing selectivity towards CA II. For reference, inhibitor **3** (gray) is depicted. C) Green contours (levels: C.2: -0.008 , C.3: -0.015 , C.ar: -0.017) indicate regions favoring CA I selectivity, orange contours (levels: C.2: 0.015 , C.3: 0.009 , C.ar: 0.025) depict areas increasing selectivity towards CA II. For reference, the inhibitors **5** (gray) and **4** (brown) are shown.



Scheme 2. Chemical formulae of the molecules mentioned in the Results and Discussion section.

AFMoC approach also exploits protein information and therefore it reveals no predominant contour, because the protein environment does not favor the presence of an O.2 atom in this region (Figure 3B). The magenta contour in the CoMSIA map depicts a CA IV selectivity-enhancing region. This area is close to the oxygen of the exocyclic sulfonamide group of the CA IV-selective thienothiopyranes (for example, **7**). In both proteins CA I and CA IV, however, the conformation and intramolecular hydrogen bond network of the neighboring Gln92 prevents the formation of a hydrogen bond to the ligand oxygen. In consequence, AFMoC does not highlight this region by a corresponding contour.

A similar behavior of the AFMoC method can be observed also in the other maps. It is interesting to note that some of

the AFMoC maps show very sharply bordered, fragmented contours, which surround single atoms of ligands. Obviously in this region the respective dependent variable adopts rather extreme values. This possibly indicates an overly steep functional form of the AFMoC potentials, and minor alignment differences with respect to these atoms are highlighted as significant if the corresponding ligands differ in their selectivity profiles. One possibility to overcome this problem may be the choice of a value greater than 0.85 (σ) for the width of the Gaussian function that maps the ligand atom types onto the distance-dependent pair potentials. This would lead to a broader “smearing” of the ligand-atom-derived weights and thus produce smoother gradients in the descriptor values.

As already described above, we investigated two alternative approaches to generate selectivity models for the three 3D QSAR methods used. One is to correlate the pK_i differences (ΔpK_i) as independent variables with the ligand or interaction fields. The other is to build separate models for two pK_i values and to calculate the differences of corresponding PLS coefficients subsequently. In latter case, however, it has to be taken into account that due to the separate derivation of the PLS models, the scale of the two subtracted coefficient maps

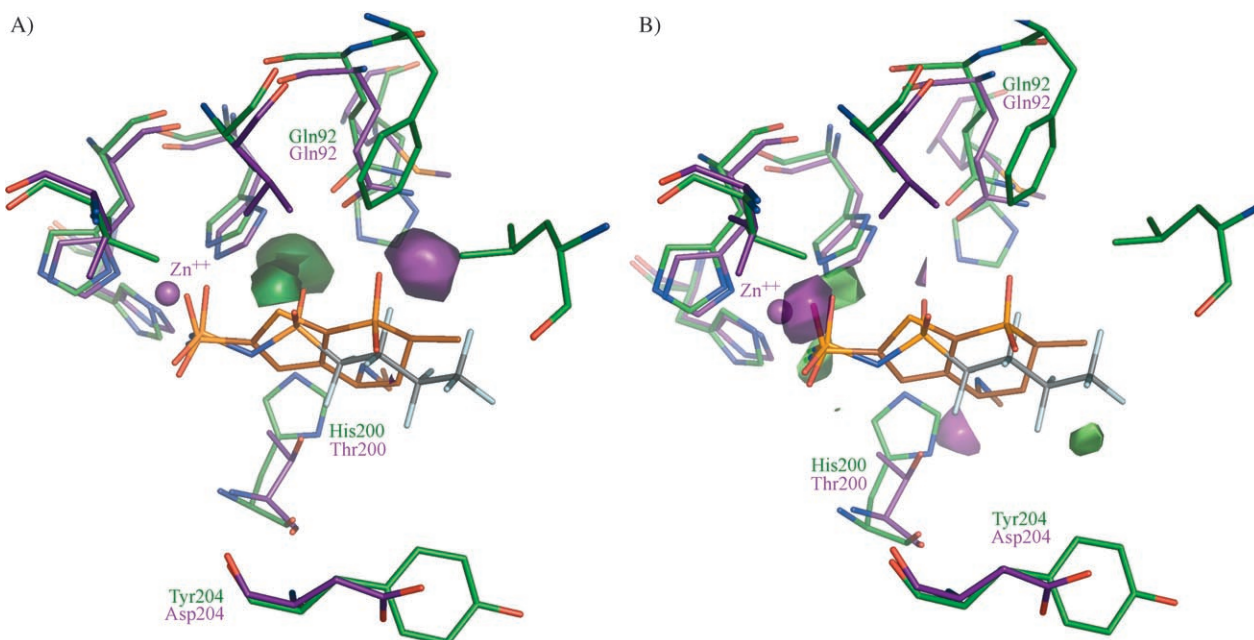


Figure 3. A) Acceptor CoMSIA and B) O.2 AFMoC stdev*coeff contour maps for CA I/IV selectivity. The catalytic zinc ion (violet sphere) is shown as well as selected amino acids of CA I (green) and CA IV (purple); hydrogen atoms are omitted for clarity. For reference, inhibitors **6** ($\Delta pK_i(I-IV) = 1.15$, gray) and **7** ($\Delta pK_i(I-IV) = -3.05$, brown) are depicted. A) Green contours (level: 0.005) indicate regions enhancing selectivity towards CA I, purple contours (level: -0.0025) show areas increasing selectivity towards CA IV. B) Green contours (level: -0.0025) indicate regions enhancing selectivity towards CA I, purple contours (level: 0.003) encapsulate areas increasing selectivity towards CA IV.

might differ. Hence, we calculated the difference maps on the unscaled as well as on normalized maps, fitted to a value range between -1 and 1 , and compared the results. Visual inspection shows that—at least in our case—the normalization does not significantly alter the contours for any of the applied QSAR techniques. The same holds true for a comparison of the maps obtained by separate PLS evaluation and a single correlation with the pK_i differences for CoMFA and CoMSIA. Due to methodological reasons in the case of AFMoC, the “separate” variant allows the inclusion of information of two different protein structures and shows significant differences compared to the use of the ΔpK_i . This is discussed in detail below.

Differential GRID maps and CPCA

At first the protein-based contouring using GRID probes are discussed. Three principal components (PC) were extracted during the derivation of the CPCA models. Table 4 shows the

PC	Consensus ^[b]	Probe			
		DRY	C3	N1	O
1	55.31	42.38	60.87	61.47	59.73
2	63.80	47.75	69.11	70.04	69.10
3	67.67	55.30	72.99	73.25	71.91

[a] Percentage of overall variance of original descriptor matrix. [b] Corresponds to a simple PCA using all probes simultaneously.

amount of variance captured in each PC on the consensus level (corresponding to an ordinary PCA with all four probes simultaneously) and on the block level (referring to a single probe). For all probes the original data structure can sufficiently be summarized by three PCs; in the case of the DRY probe, however, only approximately 55% of the variance (versus 72% for C3, N1, or O) can be explained by the first three PCs, indicating a higher degree of complexity in the underlying data structure.

Figure 4 shows the CPCA scores (block scores) plot of the O probe for the first two PCs. The overall PCA scores (consensus scores) plot as well as the block scores for the other three probes display almost identical distribution. The scores plot shows a well-defined clustering of the representatives of the three isozymes. The first PC separates the CA I class from CA II and CA IV, while the second PC discriminates CA IV from CA I and CA II. This evaluation was compared with a simple subtraction of the corresponding GRID maps.

As an example, Figure 5 shows the O probe selectivity maps for CA I/II selectivity (active differential CPCA plot, loadings). In Figure 5A regions associated with CA I selectivity are depicted together with compound **8** ($\Delta pK_i(\text{I-II}) = -2.60$, brown) for orientation. The blue meshes were derived by the CPCA approach, whereas the green solid contours were generated by building the differences of the GRID values. The region close to His67 (CA I) is marked by both approaches as important for

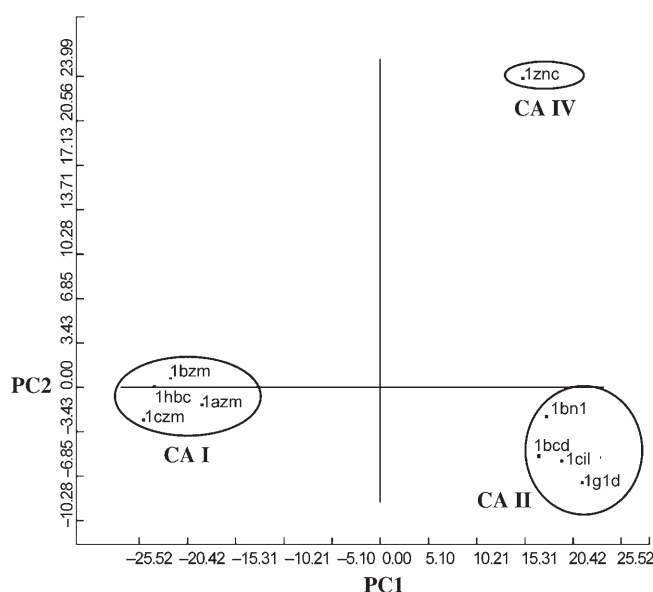


Figure 4. CPCA scores plot for the carbonyl oxygen probe. The clustering of the structures representing each isozyme is evident. PC 1 separates the CA I class from CA II and IV, whereas PC 2 discriminates CA IV from CA I and II.

CA I selectivity. Three amino acid mutations may explain the occurrence of this contour: the nitrogen atoms of His67 and His200 in CA I point directly to this area and can act as donors if a suitable tautomeric form is assumed. The respective amino acid side chains of CA II (Asn67 and Thr200) also possess donor functions, but neither the angles nor the distances to the contour would allow them to build hydrogen bonds to a carbonyl oxygen placed at this region. Furthermore, Ser65 in CA I is close to the contour while CA II lacks a similar donor functionality in a residue side chain (Ala65). The green contour next to His64 (both isozymes) is obviously a result of alignment differences. This residue (“proton-shuttle”) is known for its conformational flexibility. Thus it differs from structure to structure, and the corresponding area should be excluded from selectivity considerations. The CPCA approach, however, seems to be less sensitive to such effects, as it indicates only a very small field contribution in this region. It has to be kept in mind, though, that the “region cut-out tool” of GOLPE was solely applied to the CPCA maps; consequently, contours in the periphery will appear in differential GRID maps only, because the corresponding variables have been discarded from the input matrix of the CPCA.

Figure 5B shows the regions attributed to CA II selectivity. The solid orange contours are produced by the GRID difference method, and red meshes are generated by CPCA. Both maps are almost identical. The large contour surrounding Thr200 (CA II) and His200 (CA I) is caused by the fact that in this area a hydrogen bond to the hydroxy group of Thr200 is possible, whereas His200, the nitrogen atom of which can also operate as donor, approaches too close to this region. A similar explanation holds for the neighboring contour associated with Asn67 (CA II) and His67 (CA I). The contour close to Gln92 is produced by the occurrence of different conformations of the same amino acid in both proteins. These conformations are in-

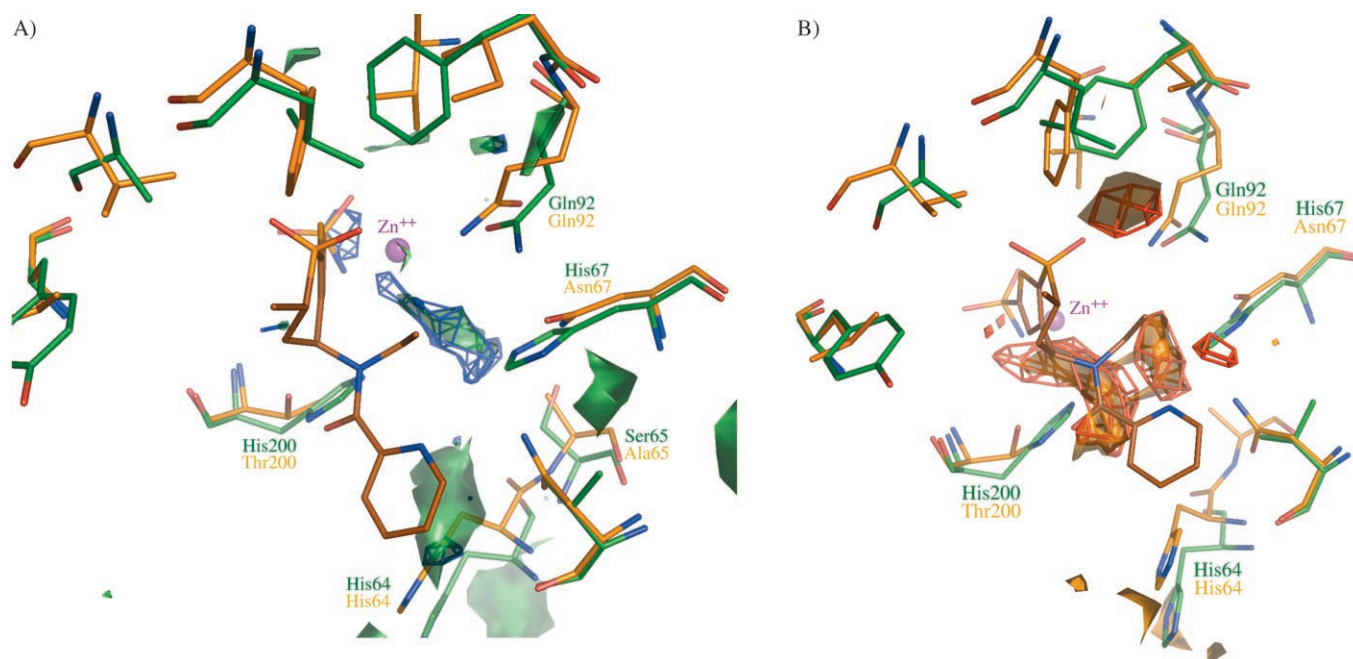


Figure 5. Protein-derived CA I/II selectivity maps obtained by CPCA and subtraction of GRID descriptors. The catalytic zinc ion (violet sphere) and selected amino acids of CA I (green) and CA II (orange) are shown. For reference, inhibitor **8** ($\Delta pK_i(\text{I-II}) = -2.60$, brown) is depicted. A) CA I selectivity contour maps. Green solid contours (level: 7.0) were generated by the difference method, whereas blue meshes (level: -2.3) were derived by the CPCA approach. B) CA II selectivity contour maps. Orange solid contours (level: -8.0) were generated by the difference method, whereas red meshes (level: 2.3) were derived by the CPCA approach.

duced by different amino acids in the vicinity of Gln92 and their respective involvement in a hydrogen bonding network to the interior of the protein: in CA I the nitrogen of Gln92 forms a hydrogen bond to Asn69 in the protein interior and thus, does not point its donor functionality into the binding pocket. In contrast, in CA II the neighboring amino acid 69 is a glutamic acid that forms a bidentate salt bridge to Arg58, and it is hence unable to accept a hydrogen bond from Gln92. Consequently, Gln92 possesses an unsatisfied donor functionality that can be involved in binding. The corresponding carbonyl acceptor oxygen of the terminal amide group of Gln92 is engaged either in CA I and II in a hydrogen bond to the neighboring His94.

This comparison exemplarily shows that the use of differential GRID maps for the extraction of protein-based selectivity information is an alternative way to the well-known CPCA approach. In our case, the maps of both methods show no significant differences. However, the advantage of CPCA is that it provides insight into the relationships between the studied proteins in terms of scores plots. Furthermore, it evaluates rather principle components than raw data, which should result in a reduction of noise likely contained in the descriptor matrix.

Synopsis of the approaches

So far in this study, three methodologically different approaches have been presented to unravel selectivity-determining features. In the following section, we compare their results to feature the major differences.

Figure 6 shows the contour maps for CoMSIA (6A, acceptor field), AFMoC (6B, O.2 field, orange solid contours: separate PLS method using two proteins, red meshes: PLS based on ΔpK_i using CA II (1cil) as reference only). In Figure 6C differential GRID fields are presented (O field) to trace selectivity differences between CA I and II. For all contours the presence of the respective probe enhances selectivity for CA II in the highlighted region. For orientation, the CA II-selective inhibitor **8** ($\Delta pK_i(\text{I-II}) = -2.60$, brown) is also depicted.

The contours next to the zinc anchor, present either in the CoMSIA and AFMoC maps, are difficult to interpret and probably result as a consequence of slight alignment differences of the ligands. The large CoMSIA contour on the right of residue 200 (CA I: His, CA II: Thr) is evoked by the carbonyl or sulfonyl oxygen present in some potent *para*-amino-substituted phenylsulfonamides showing CA II preference. This contour only reflects the empirically observed trend that ligands with an acceptor function at this position possess on average higher affinity for CA II, but no structural reason (such as a donor function in CA II that is not present in CA I) can be encountered in the receptor structures. Accordingly, the purely protein-based differential maps produced by GRID do not show a CA II selectivity-enhancing region in this area. In the case of AFMoC (Figure 6B), the presence of a contour depends on the way the models were derived: if only one protein structure (CA II) is considered, and PLS is performed with respect to ΔpK_i values as dependent variables (red meshes), the contour observed in CoMSIA is also indicated. If the map is constructed by evaluating the differences of the $\text{stdev} \times \text{coeff}$ from separately generated models including both protein structures (CA I and CA II),

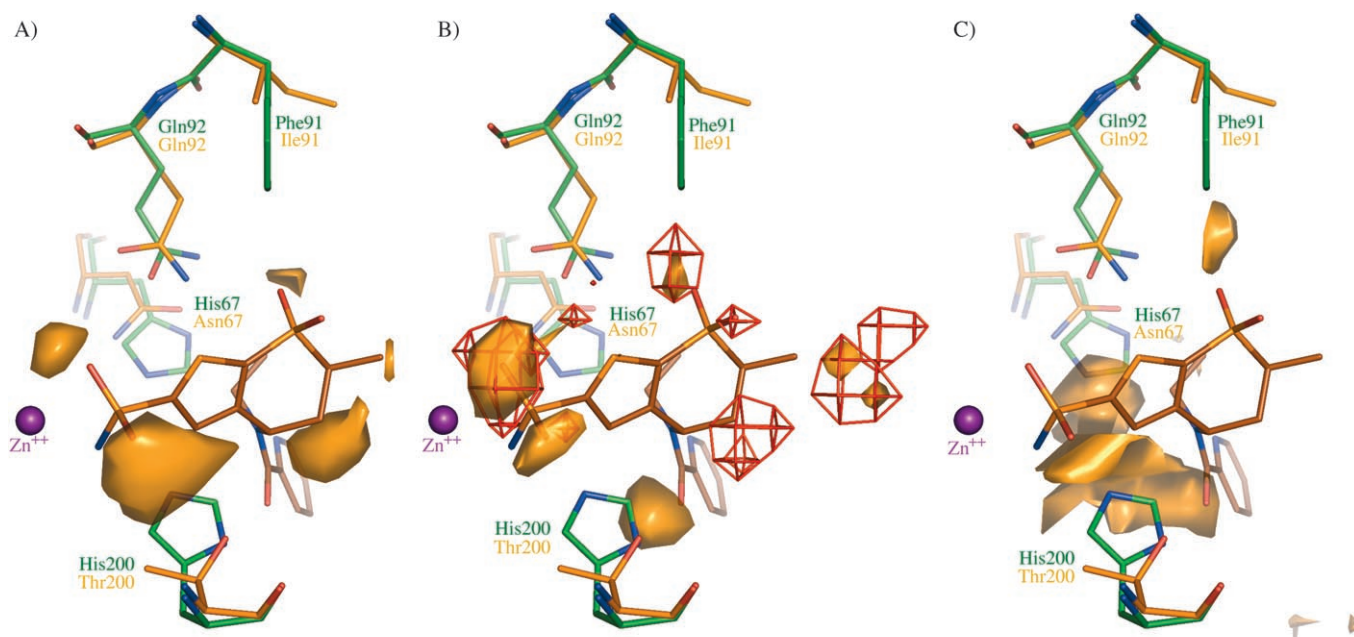


Figure 6. Synopsis of the A) CoMSIA-, B) AFMoC-, and C) GRID-based CA I/II selectivity maps. The catalytic zinc ion (violet sphere) as well as selected amino acids of CA I (green) and CA II (orange) are depicted; hydrogen atoms are omitted for clarity. For reference, inhibitor **8** ($\Delta pK_i(\text{I-II}) = -2.60$, brown) is shown. All depicted contours indicate areas enhancing selectivity for CA II. A) CoMSIA stdev*coeff acceptor map (level: -0.0023). B) AFMoC stdev*coeff O.2 maps. The solid orange contours (level: 0.002) were generated by building individual models for CA I and II and using both proteins. The red meshes (level: 0.002) were produced by PLS analysis with $\Delta pK_i(\text{I-II})$ as dependent variable and only CA II as protein. C) GRID differential O maps (level: -8.0), generated by subtraction of corresponding grid points without normalization.

the region is not detected as significant. This can be explained by the fact that the former methodological variant considers the selectivity information through ligand information only (in terms of affinity differences data), whereas the latter approach additionally exploits the differences in the protein environments. Analogously, the red meshes to the very right in the AFMoC ΔpK_i map highlight an area where a few ligands with moderate CA II preference place their O.2 atoms. Since this trend is not very pronounced, the CoMSIA map (Figure 6A) exhibits there only a very tiny contour. In the AFMoC contour map originating from two proteins (Figure 6B, solid contour), the contour is also strongly reduced taking into account that only the ligand information substantiates the presence of such a contour while the protein structures show no obvious reason for it. Accordingly, the differential GRID maps (Figure 6C) also lack a corresponding contour. The solid-orange AFMoC contour in the direct vicinity (right) of His/Thr200 gives an example of the inverse case where the receptor environment produces a contour which is absent if ligand information is considered only. As indicated by the large orange differential GRID contour (Figure 6C), the presence of an oxygen acceptor is favorable for CA II selectivity at this position due to the hydroxy group of Thr200, which is replaced by a histidine residue in CA I. Several CA II-selective inhibitors with a thienothiopyrane scaffold (such as **8**) possess an O.2 atom in this region. Obviously, this ligand information is not sufficient to produce a contour, since neither the CoMSIA nor the single-protein AFMoC maps (red meshes) contour this region as important

for CA II selectivity. However, the AFMoC approach using two protein structures (solid-orange contour) seems to enhance the ligand-based information with additional knowledge about differences in the considered protein structures, thus producing that contour. A particularly interesting case are the contours around the endocyclic sulfone group of **8**. Considering only protein information, the presence of one contour near Gln92 is expected, as explained above. This contour is found in the maps of all approaches used herein. A contour around the second oxygen atom (not involved in hydrogen bonding to Gln92) would be reasonable only from the point of view of the ligands, because all ligands with that thienothiopyrane structure exhibit strong selectivity towards CA II. This difference can clearly be seen evaluating the maps of both AFMoC variants (Figure 6B). The AFMoC model utilizing only one protein reveals red meshes at both oxygen atoms, whereas the model including information of both proteins generates only one contour at the oxygen next to Gln92 which is in accordance with differences in the receptor structures (see above).

One area near His/Asn67 is contoured by the differential GRID approach only (Figure 6C). Since this region is not occupied by any of the ligands in the considered dataset, none of the 3D QSAR methods identifies this region as important for CA II selectivity. Therefore, it is always advisable to also consult purely protein-based approaches as supplement, if possible.

This comparison demonstrates that the AFMoC approach highlights regions as important for selectivity similar to those also marked by the ligand-based CoMSIA approach. However,

the AFMoC contours are partly modified according to the differences in the receptor structures, either generating additional contours or diminishing the ligand-based contours.

Conclusions

The optimization of lead structures does not only require the enhancement in terms of their affinity; the elaboration of a satisfactory selectivity profile is also of utmost importance in order to avoid undesired side effects. In this study, we selected the carbonic anhydrases I, II, and IV as an example, as insufficient selectivity of inhibitors can produce serious problems due to pronounced similarity of these isozymes. A large high-quality dataset was used to derive statistically significant and predictive 3D QSAR (CoMFA, CoMSIA) models to quantitatively estimate affinity and selectivity data. The interpretation of the contour maps is consistent with relationships found for spatial properties of the inhibitors and the trends of the data to predict. However, since these methods solely exploit ligand information, the contours resembled only in part the requirements and differences defined by the protein structures. To supplement the analyses also with protein information, the binding sites were examined with GRID on the one hand, and AFMoC models were generated on the other hand. The developed models can be used for further design in two ways: the contour maps provide hints for possible structural modifications, while the QSAR equations can be used to predict the binding properties within inhibitor series, for example, of focused combinatorial libraries, particularly if they are designed in a way that they do not extrapolate beyond the applicability domain defined by the employed models.

In summary, the following amino acid residues are most probably determinant to be considered for design of selective inhibitors: His200 is only present in CA I, whereas a threonine constitutes the corresponding residue in CA II and IV. The introduction of sterically demanding substituents into potential ligands close to this residue will enhance selectivity towards CA II and IV. If the substitutions additionally exhibit an acceptor function that can form a hydrogen bond to the hydroxy group of the threonine, the selectivity increase can even be enhanced. To achieve an opposing selectivity profile, the same histidine residue can be addressed by a sterically confined acceptor function. This group can further interact with His67 (CA II: Asn67; CA IV: Met67) and Ser65 (CA II: Ala65; CA IV: Ser65), present in CA I, to enhance selectivity towards CA I. Since CA IV, but not CA II (Ala65), possesses a serine at position 65 too, a similar substitution might be used to increase selectivity towards CA IV relative to CA I or II. Furthermore, the static differences of the conformations of Gln92 due to deviating hydrogen bond networks could be exploited for the design of CA II-selective inhibitors by introduction of a suitable acceptor function. Eventually, the steric differences next to the residues 91 and 131 could also be exploited to favor selectivity either towards CA I or II. But due to the small distance between these residues and their inverse steric demands (CA I: Phe91/Leu131; CA II: Ile91/Phe131) an appropriate chemical modification of an inhibitor targeting only the properties of

one of these residues will be difficult. Further options for the design of selective inhibitors can be deduced from the other contours discussed in the synopsis section, even if they are not directly linked to the differences of an amino acid exchange in the active sites. They empirically reflect correlations between structural differences of the ligands and their achieved affinities/selectivities. Thus they may provide valuable guidelines how to perform ligand modification, though not intimately explainable by one particular spot in the protein structures.

The comparison of the different contour maps underlines the complementary character of ligand- and protein-based approaches and demonstrates the capability of AFMoC to efficiently combine both sources of information.

Acknowledgements

The authors are grateful to Dr. Christoph A. Sotriffer for constructive discussions and critical review of the manuscript.

Keywords: 3D QSAR • AFMoC • carbonic anhydrase • CoMFA • CoMSIA • CPCA

- [1] S. Lindskog, *Pharmacol. Ther.* **1997**, *74*, 1–20.
- [2] T. H. Maren, *Physiol. Rev.* **1967**, *47*, 595–781.
- [3] C. Geers, G. Gros, *Physiol. Rev.* **2000**, *80*, 681–715.
- [4] C. T. Supuran, A. Scozzafava, *Curr. Med. Chem. Immunol. Endocr. Metab. Agents* **2001**, *1*, 61–97.
- [5] C. T. Supuran, F. Briganti, S. Tilli, W. R. Chegwidden, A. Scozzafava, *Bioorg. Med. Chem.* **2001**, *9*, 703–714.
- [6] C. T. Supuran, *Expert Opin. Ther. Pat.* **2000**, *10*, 575–600.
- [7] C. T. Supuran, A. Scozzafava, A. Casini, *Med. Res. Rev.* **2003**, *23*, 146–189.
- [8] R. D. Cramer, *J. Am. Chem. Soc.* **1988**, *110*, 5959–5967.
- [9] G. Klebe, U. Abraham, T. Mietzner, *J. Med. Chem.* **1994**, *37*, 4130–4146.
- [10] S. Wold, E. Johansson, M. Cocchi in *3D QSAR in Drug Design: Theory Methods and Applications*, Vol. 1 (Ed.: H. Kubinyi), ESCOM, Leiden, **1993**, pp. 523–550.
- [11] G. Wong, K. F. Koehler, P. Skolnick, Z. Q. Gu, S. Ananthan, P. Schonholzer, W. Hunkeler, W. Zhang, J. M. Cook, *J. Med. Chem.* **1993**, *36*, 1820–1830.
- [12] M. Böhm, J. Stürzebecher, G. Klebe, *J. Med. Chem.* **1999**, *42*, 458–477.
- [13] H. Matter, W. Schwab, *J. Med. Chem.* **1999**, *42*, 4506–4523.
- [14] A. Agarwal, P. P. Pearson, E. W. Taylor, H. B. Li, T. Dahlgren, M. Herslof, Y. Yang, G. Lambert, D. L. Nelson, J. W. Regan, A. R. Martin, *J. Med. Chem.* **1993**, *36*, 4006–4014.
- [15] R. E. Wilcox, T. Tseng, M. Y. Brusniak, B. Ginsburg, R. S. Pearlman, M. Teeter, C. DuRand, S. Starr, K. A. Neve, *J. Med. Chem.* **1998**, *41*, 4385–4399.
- [16] R. E. Wilcox, W. H. Huang, M. Y. Brusniak, D. M. Wilcox, R. S. Pearlman, M. M. Teeter, C. J. DuRand, B. L. Wiens, K. A. Neve, *J. Med. Chem.* **2000**, *43*, 3005–3019.
- [17] J. A. Moron, M. Campillo, V. Perez, M. Unzeta, L. Pardo, *J. Med. Chem.* **2000**, *43*, 1684–1691.
- [18] P. J. Goodford, *J. Med. Chem.* **1985**, *28*, 849–857.
- [19] P. Goodford, *GRID version 22a for Linux* (Molecular Discovery Ltd.): Oxford (UK) **2004**.
- [20] M. A. Kastenholz, M. Pastor, G. Cruciani, E. E. Haaksma, T. Fox, *J. Med. Chem.* **2000**, *43*, 3033–3044.
- [21] S. Clementi, GOLPE 4.5, Multivariate Informatic Analysis (MIA): Viale dei Castagni 16, Perugia (Italy) **1999**.
- [22] H. Gohlke, G. Klebe, *J. Med. Chem.* **2002**, *45*, 4153–4170.
- [23] K. Silber, P. Heidler, T. Kurz, G. Klebe, *J. Med. Chem.* **2005**, *48*, 3547–3563.
- [24] H. Matter, D. W. Will, M. Nazare, H. Schreuder, V. Laux, V. Wehner, *J. Med. Chem.* **2005**, *48*, 3290–3312.
- [25] H. Gohlke, M. Hendlich, G. Klebe, *J. Mol. Biol.* **2000**, *295*, 337–356.

- [26] H. Gohlke, G. Klebe, *Angew. Chem.* **2002**, *41*, 2764–2798; *Angew. Chem. Int. Ed.* **2002**, *41*, 2644–2676.
- [27] H. Gohlke, G. Klebe, *Curr. Opin. Struct. Biol.* **2001**, *11*, 231–235.
- [28] C. A. Sotriffer, H. Gohlke, G. Klebe, *J. Med. Chem.* **2002**, *45*, 1967–1970.
- [29] H. Gohlke, M. Hendlich, G. Klebe, *Perspect. Drug Discovery Des.* **2000**, *20*, 115–144.
- [30] D. W. Christianson, J. D. Cox, *Annu. Rev. Biochem.* **1999**, *68*, 33–57.
- [31] S. Lindskog, J. E. Coleman, *Proc. Natl. Acad. Sci. USA* **1973**, *70*, 2505–2508.
- [32] F. Abbate, C. T. Supuran, A. Scozzafava, P. Orioli, M. T. Stubbs, G. Klebe, *J. Med. Chem.* **2002**, *45*, 3583–3587.
- [33] C. K. Tu, D. N. Silverman, C. Forsman, B. H. Jonsson, S. Lindskog, *Biochemistry* **1989**, *28*, 7913–7918.
- [34] C. Tu, M. Qian, J. N. Earnhardt, P. J. Laipis, D. N. Silverman, *Biophys. J.* **1998**, *74*, 3182–3189.
- [35] SYBYL molecular modeling package, Tripos Inc., 1699 South Hanley Road, Suite 303, St. Louis, MO 63144 (USA) **2005**.
- [36] W. L. DeLano, The PyMOL Molecular Graphics System, DeLano Scientific, San Carlos, CA (USA) **2005**.
- [37] A. Golbraikh, M. Shen, Z. Xiao, Y. D. Xiao, K. H. Lee, A. Tropsha, *J. Comput.-Aided Mol. Des.* **2003**, *17*(2–4), 241–253.
- [38] R. D. Clark, *J. Chem. Inf. Comput. Sci.* **1997**, *37*, 1181–1188.
- [39] R. D. Clark, *J. Chem. Inf. Comput. Sci.* **1998**, *38*, 1079–1086.
- [40] A. Weber, PhD Thesis, Philipps-Universität Marburg (Germany) **2004**.
- [41] U. Thibaut, G. Folkers, G. Klebe, H. Kubinyi, A. Merz, D. Rognan in *3D QSAR in Drug Design: Theory Methods and Applications, Vol. 1* (Ed.: H. Kubinyi), ESCOM, Leiden, **1993**, pp. 711–716.
- [42] C. T. Supuran, A. Scozzafava, L. Menabuoni, F. Mincione, F. Briganti, G. Mincione, *Eur. J. Pharm. Sci.* **1999**, *8*, 317–328.
- [43] C. T. Supuran, *Eur. J. Med. Chem.* **1999**, *34*, 799–808.
- [44] L. Menabuoni, A. Scozzafava, F. Mincione, F. Briganti, G. Mincione, C. T. Supuran, *J. Enzyme Inhib.* **1999**, *14*, 457–474.
- [45] A. Popescu, A. Simion, A. Scozzafava, F. Briganti, C. T. Supuran, *J. Enzyme Inhib.* **1999**, *14*, 407–423.
- [46] A. Scozzafava, C. T. Supuran, *J. Enzyme Inhib.* **1999**, *14*, 343–363.
- [47] A. Scozzafava, L. Menabuoni, F. Mincione, F. Briganti, G. Mincione, C. T. Supuran, *J. Med. Chem.* **2000**, *43*, 4542–4551.
- [48] C. T. Supuran, A. Scozzafava, *Eur. J. Med. Chem.* **2000**, *35*, 867–874.
- [49] C. T. Supuran, *Eur. J. Med. Chem.* **1998**, *33*, 577–594.
- [50] M. Ilies, C. T. Supuran, A. Scozzafava, A. Casini, F. Mincione, L. Menabuoni, M. T. Caproiu, M. Maganu, M. D. Banciu, *Bioorg. Med. Chem.* **2000**, *8*, 2145–2155.
- [51] A. Casini, A. Scozzafava, F. Mincione, L. Menabuoni, M. A. Ilies, C. T. Supuran, *J. Med. Chem.* **2000**, *43*, 4884–4892.
- [52] A. Casini, A. Scozzafava, F. Mincione, L. Menabuoni, C. T. Supuran, *J. Enzyme Inhib. Med. Chem.* **2002**, *17*, 333–343.
- [53] A. Scozzafava, F. Mincione, L. Menabuoni, C. T. Supuran, *Drug Des. Discovery* **2001**, *17*, 337–348.
- [54] F. Mincione, M. Starnotti, L. Menabuoni, A. Scozzafava, A. Casini, C. T. Supuran, *Bioorg. Med. Chem. Lett.* **2001**, *11*, 1787–1791.
- [55] B. Masereel, S. Rolin, F. Abbate, A. Scozzafava, C. T. Supuran, *J. Med. Chem.* **2002**, *45*, 312–320.
- [56] C. T. Supuran, A. Scozzafava, M. A. Ilies, F. Briganti, *J. Enzyme Inhib.* **2000**, *15*, 381–401.
- [57] G. Renzi, A. Scozzafava, C. T. Supuran, *Bioorg. Med. Chem. Lett.* **2000**, *10*, 673–676.
- [58] G. Mincione, L. Menabuoni, F. Briganti, F. Mincione, A. Scozzafava, C. T. Supuran, *Eur. J. Pharm. Sci.* **1999**, *9*, 185–199.
- [59] C. T. Supuran, F. Briganti, L. Menabuoni, G. Mincione, F. Mincione, A. Scozzafava, *Eur. J. Med. Chem.* **2000**, *35*, 309–321.
- [60] A. Scozzafava, F. Briganti, G. Mincione, L. Menabuoni, F. Mincione, C. T. Supuran, *J. Med. Chem.* **1999**, *42*, 3690–3700.
- [61] M. Barboiu, C. T. Supuran, L. Menabuoni, A. Scozzafava, F. Mincione, F. Briganti, G. Mincione, *J. Enzyme Inhib.* **2000**, *15*, 23–46.
- [62] A. Scozzafava, L. Menabuoni, F. Mincione, F. Briganti, G. Mincione, C. T. Supuran, *J. Med. Chem.* **1999**, *42*, 2641–2650.
- [63] J. Borras, A. Scozzafava, L. Menabuoni, F. Mincione, F. Briganti, G. Mincione, C. T. Supuran, *Bioorg. Med. Chem.* **1999**, *7*, 2397–2406.
- [64] C. T. Supuran, A. Scozzafava, *J. Enzyme Inhib.* **2000**, *15*, 597–610.
- [65] A. Scozzafava, C. T. Supuran, *Bioorg. Med. Chem. Lett.* **2000**, *10*, 1117–1120.
- [66] A. Scozzafava, M. D. Banciu, A. Popescu, C. T. Supuran, *J. Enzyme Inhib.* **2000**, *15*, 533–546.
- [67] C. T. Supuran, A. Scozzafava, B. C. Jurca, M. A. Ilies, *Eur. J. Med. Chem.* **1998**, *33*, 83–93.
- [68] A. Scozzafava, C. T. Supuran, *J. Med. Chem.* **2000**, *43*, 3677–3687.
- [69] A. Scozzafava, M. D. Banciu, A. Popescu, C. T. Supuran, *J. Enzyme Inhib.* **2000**, *15*, 443–453.
- [70] G. Klebe in *3D QSAR in Drug Design: Theory Methods and Applications, Vol. 1* (Ed.: H. Kubinyi), ESCOM, Leiden, **1993**, pp. 173–199.
- [71] C. Lemmen, T. Lengauer, *J. Comput.-Aided Mol. Des.* **2000**, *14*, 215–232.
- [72] RCSB, Protein Data Bank from the Research Collaboratory for Structural Bioinformatics; <http://www.rcsb.org/>
- [73] H. M. Berman, J. Westbrook, Z. Feng, G. Gilliland, T. N. Bhat, H. Weissig, I. N. Shindyalov, P. E. Bourne, *Nucleic Acids Res.* **2000**, *28*, 235–242.
- [74] S. Grüneberg, M. T. Stubbs, G. Klebe, *J. Med. Chem.* **2002**, *45*, 3588–3602.
- [75] J. Gasteiger, C. Rudolph, J. Sadowski, *Tetrahedron Comput. Methodol.* **1990**, *3*, 537–547.
- [76] J. Gasteiger, M. Marsili, *Tetrahedron* **1980**, *36*, 3219–3228.
- [77] M. Clark, R. D. Cramer, N. van Opdenbosch, *J. Comput. Chem.* **1989**, *10*, 982–1012.
- [78] P. R. Gerber, K. Müller, *J. Comput.-Aided Mol. Des.* **1995**, *9*, 251–268.
- [79] B. L. Bush, R. B. Nachbar, Jr., *J. Comput.-Aided Mol. Des.* **1993**, *7*, 587–619.
- [80] R. D. Cramer, S. A. DePriest, D. E. Patterson, P. Hecht in *3D QSAR in Drug Design: Theory Methods and Applications, Vol. 1* (Ed.: H. Kubinyi), ESCOM, Leiden, **1993**, pp. 443–485.
- [81] T. Naumann, H. Matter, *J. Med. Chem.* **2002**, *45*, 2366–2378.
- [82] T. I. Oprea, C. L. Waller in *Reviews in Computational Chemistry, Vol. 11* (Eds.: K. B. Lipkowitz, D. B. Boyd), Wiley, New York, **1997**, pp. 127–182.
- [83] G. Klebe, U. Abraham, *J. Med. Chem.* **1993**, *36*, 70–80.
- [84] A. M. Doweiko, *J. Comput.-Aided Mol. Des.* **2004**, *18*, 587–596.
- [85] A. Golbraikh, A. Tropsha, *J. Mol. Graphics Modell.* **2002**, *20*, 269–276.

Received: March 30, 2006

Published online on July 10, 2006